Time-Delay Identification and Validation of a Liquid Film Transport Model based on Pilot Plant Experiments ⋆

Julian Hofmann * **Anton Ponomarev** ** **Veit Hagenmeyer** * **Lutz Gröll** *

* *Karlsruhe Institute of Technology, Hermann-von-Helmholtz-Platz 1, 76344 Eggenstein-Leopoldshafen, Germany (e-mail: julian.hofmann@kit.edu).*
** *Saint Petersburg State University, Department of Mechanics of Controlled Motion, 7/9 Universitetskaya nab., 199034 St. Petersburg, Russia (e-Mail: a.ponomarev@spbu.ru)*

Abstract: The paper presents an identification strategy to obtain relations between time delays of a transport model for an evaporating liquid film and corresponding flow/liquid properties. To this end, step-response based pilot plant experiments referring to the falling film evaporator process are conducted. In this context, the time-delay relations are identified offline by minimizing the output error between the model and experiment. In subsequent validation experiments, we observe that modeled and measured outputs are in good accordance. Within this framework, we conclude that the influence of evaporation on the liquid's time-delay behavior can be neglected.

Keywords: Time Delay, Modeling, Identification, Validation, Falling Film Evaporator

1. INTRODUCTION

In chemical and process engineering applications, transport modeling is of basic interest for control and simulation. Therefore, fundamental balance equations of mass, momentum or energy are formulated and commonly lead to systems of partial differential equations (PDEs) (Van Genuchten (1982)). However, detailed PDE-based models often require large computational effort (Kharangate et al. (2015); Donaldson and Thimmaiah (2016)) and are difficult to handle for control design due to their complexity. To mitigate these limitations, a modern approach consists in modeling hyperbolic PDEs and transforming them via the method of characteristics into time-delay equations (Witrant and Niculescu (2010); Karafyllis and Krstic (2014); Bresch-Pietri and Petit (2016)). Recently, the authors applied this approach to develop novel transport models for liquid films in tubes (Hofmann et al. (2020)) and additionally considered evaporation (Ponomarev et al. (2020)).

The practical background of this research is the falling film evaporator (FFE) process (Paramalingam (2004); Winchester (2000)). Operation and control of this process is challenging due to dominant time delays (Schwaer et al. (2020)), which are induced by liquid transport. While completely filled pipes can essentially be modeled by constant or time-varying transport delays (Zhang and Yeddanapudi (2012); Zenger and Ylinen (1994)), the dynamic behavior of falling liquid film is complex due to many overlapping physical phenomena (Craster and Matar (2009); Keyhani (2001)). Thus, in (Hofmann et al. (2020); Ponomarev et al. (2020)), the authors introduced the *Overtaking Particle Flow* (OPF) model. On the one hand, the latter is simple enough to serve for control design but on the other hand, it should be able to adequately map the dynamics of evaporating falling liquid films. Consequently, identification and validation of the OPF model are required. Corresponding results are presented in this contribution.

Hence, we design pilot plant experiments to identify the time delays of the OPF model. Regarding FFE tubes, there exist lots of experimental studies identifying relations for liquid film thickness and heat transfer coefficients (Al-Sibai (2006); Åkesjö (2018); Karapantsios and Karabelas (1995)) but, to the best of our knowledge, no results on time-delay relations are available. To fill this gap, we apply step-response based pilot plant experiments *without evaporation* and use a standard output error based algorithm to identify relations between OPF time delays and flow/liquid properties offline. Subsequently, we apply these relations in validation experiments *with evaporation* showing that the OPF model describes the measured dynamic behavior well. Therefore, a further result of the present paper is that the influence of evaporation on the liquid film's time-delay behavior is negligible.

The plan of the paper is as follows. In Sec. 2, we explain the experimental set-up while corresponding model equations are introduced in Sec. 3. Sections 4 and 5 present our main result, namely identification of time-delay relations and validation of our model. In Sec. 6, we sum up our results.

⋆ The authors thank GEA Wiegand GmbH for financial support and for providing data used in this paper.

Table 1. Symbol and subscript nomenclature

Symbols		Units
A	cross-sectional area	m^2
c	velocity	$\mathrm{m\,s}^{-1}$
c_p	specific heat capacity	$\mathrm{J\,kg}^{-1}\,\mathrm{K}^{-1}$
d	inner diameter of Tube	m
g	gravity acceleration	$\mathrm{m\,s}^{-2}$
h	filling level	m
Δh_v	enthalpy of evaporation	$\mathrm{J\,kg}^{-1}$
k	heat transfer coefficient	$\mathrm{W\,m}^{-2}\,\mathrm{K}^{-1}$
ℓ	length	m
$\dot{m}$	mass flow	$\mathrm{kg\,h}^{-1}$
M	mass	kg
p	pressure	$\mathrm{kg\,m}^{-1}\,\mathrm{s}^{-2}$
Re	Reynolds number	–
w	dry matter content	$\mathrm{kg\,kg}^{-1}$
η	dynamic viscosity	mPa s
ϑ	temperature	°C
ϱ	volumetric mass density	$\mathrm{kg\,m}^{-3}$
τ	time delay	s

Subscripts	
0	initial value
f	filter
fsh	flash evaporation
H	Heat Chamber
i	input
liq	liquid
max	maximum
min	minimum
o	output
P	Plate
R	Reservoir
T	Tube
v	vapor
w	water

2. EXPERIMENTAL SET-UP

In the following, the experimental set-up is explained. Throughout the paper, we use the nomenclature given in Table 1.

2.1 Pilot Plant Description

The principle of the pilot plant is shown in Fig. 1, where the switch represents switching between circulation and single pass mode, which is detailed in Sec. 2.2 and Sec. 2.3, resp. In both modes, the liquid, dextrose with polyvinylpyrrolidone, is induced onto the Plate which distributes it such that a thin film forms on top of the Tube. When entering the Plate, flash evaporation can occur, i.e., a small amount of liquid evaporates as it undergoes a reduction in pressure. Subsequently, the liquid film flows down the inner surface of the Tube and, in case of evaporation, live steam is introduced into the Heat Chamber, i.e., to the outside Tube surface. Via condensation, the live steam provides its enthalpy of evaporation and thus triggers evaporation of the liquid film inside the Tube. Consequently, the liquid's dry matter content is increased. To ensure evaporation at low temperatures, partial vacuum is generated inside and outside the Tube. From the bottom of the Tube, the liquid flows into the Reservoir and the vapor, which comes from the liquid film, is gathered by the Condensation System. A downstream pump conveys

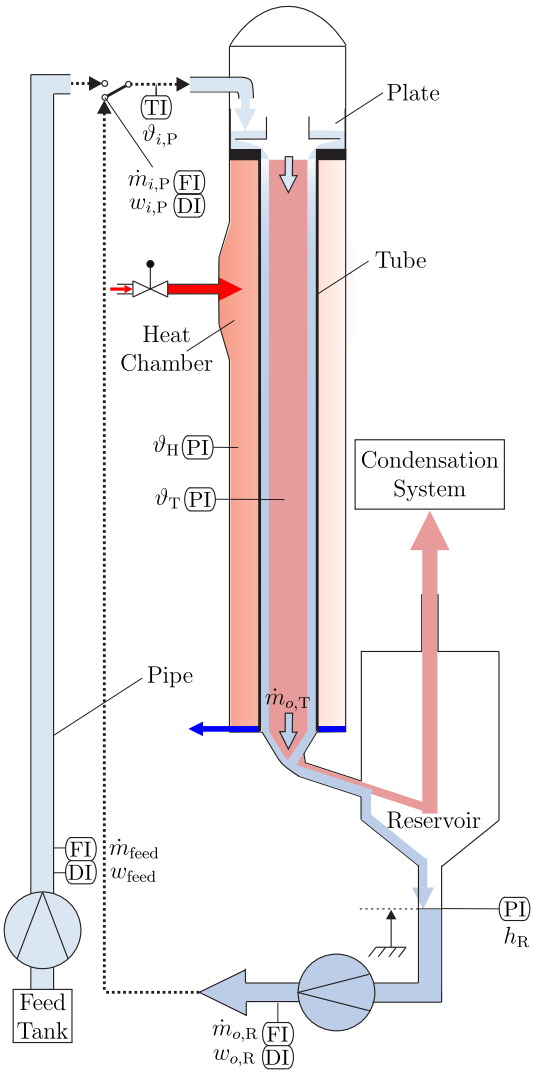

Fig. 1. Scheme of the pilot plant: The labels FI, DI, TI, and PI correspond to flow, density, temperature, and pressure identification.

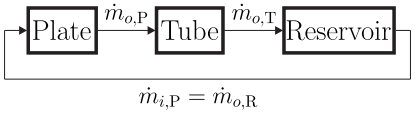

Fig. 2. Pilot plant in circulation mode

the liquid either back to the Plate (circulation) or out of the plant into some tank (single pass).

Note that all quantities shown in Fig. 1 are either directly or indirectly measured. Thereby, mass flows $\dot{m}$ are directly measured via Coriolis flow meters. Dry matter contents w are indirectly measured via temperatures ϑ and densities ϱ, see App. A. Temperatures ϑ_{T}, ϑ_{H} are indirectly measured via corresponding steam pressures. The level h_{R} is indirectly measured by the hydrostatic pressure $p_{\mathrm{R}} = \varrho_{o,\mathrm{R}} g h_{\mathrm{R}}$.

2.2 Circulation

The flow diagram of the pilot plant in circulation mode is sketched in Fig. 2. When operating in this mode, $\dot{m}_{i,\mathrm{P}}$ and $w_{i,\mathrm{P}}$ are measured on the top, right before the liquid enters the Plate. Moreover, there is neither partial

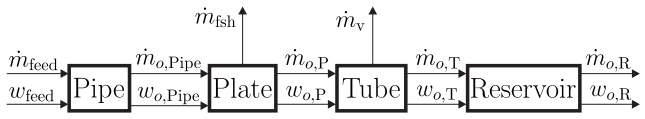

Fig. 3. Pilot plant in single pass mode

vacuum generated nor live steam induced which leads to *no evaporation*, i.e., $\dot{m}_{\text{fsh}} = \dot{m}_{\text{v}} \equiv 0$ such that dry matter content, density, and dynamic viscosity of the liquid stay constant. Thus, this operation mode enables *identification* of time delays at constant dynamic viscosity and varying mass flows, see Sec. 4. Since the dry matter content w stays constant in this mode, the mass flow $\dot{m}$ is the only relevant transport quantity. As described in Sec. 3.1, the Pipe is a feedthrough w.r.t. mass flow and therefore does not need to be considered in Fig. 2.

2.3 Single Pass

The real FFE is usually operated in single pass mode, which is depicted in Fig. 3. In this mode, $\dot{m}_{\text{feed}}$ and w_{feed} are measured at the bottom, right after the pump conveying the liquid through the Pipe from the Feed Tank to the Plate. Furthermore, live steam induction and partial vacuum generation are both active, which yields *evaporation*, i.e., $\dot{m}_{\text{v}} > \dot{m}_{\text{fsh}} > 0$. Hence, dry matter content, density, and dynamic viscosity of the liquid increase when it flows down the Tube. Due to these realistic circumstances, this operation mode is used for *validation* of the model. While the model is introduced in Sec. 3, the validation results are described in Sec. 5. Finally, note that besides mass flow $\dot{m}$, the dry matter content w is an additional transported quantity in this mode since evaporation is active.

3. MODEL

The models for the operation modes presented in Sec. 2.2 and Sec. 2.3 consist of different modules. Here, the reader should especially focus on the Tube module in Sec. 3.3 since it introduces the delays of the OPF model to be identified in Sec. 4. For brevity, we compactly describe each module by its input-output relations w.r.t. mass flow $\dot{m}$ and dry matter content w. The reader is referred to (Schwaer et al. (2020); Hofmann et al. (2020); Ponomarev et al. (2020)) for detailed derivations and calculations.

3.1 Pipe

The Pipe is modeled as feedthrough w.r.t. mass flow and variable transport delay w.r.t. dry matter content (Schwaer et al. (2020); Zhang and Yeddanapudi (2012)), i.e., its input-output relations are determined by

$$\dot{m}_{o,\text{Pipe}}(t) = \dot{m}_{i,\text{Pipe}}(t) \tag{1}$$

for the mass flow,

$$w_{o,\text{Pipe}}(t) = w_{i,\text{Pipe}}(t - \tau_{\text{Pipe}}(t)) \tag{2}$$

for the dry matter content, and

$$\frac{\mathrm{d}}{\mathrm{d}t}\tau_{\text{Pipe}}(t) = 1 - \frac{\bar{c}_{i,\text{Pipe}}(t)}{\bar{c}_{i,\text{Pipe}}(t) - \tau_{\text{Pipe}}(t)}, \tag{3a}$$

$$\tau_{\text{Pipe}}(t_f) = t_f - t_0 \tag{3b}$$

for the time delay, where t_f is calculated via the implicit relation

$$\int_{t_0}^{t_f} \bar{c}_{i,\text{Pipe}}(\theta)\,\mathrm{d}\theta = \ell_{\text{Pipe}}. \tag{4}$$

The average input velocity $\bar{c}_{i,\text{Pipe}}(t)$ is obtained by

$$\bar{c}_{i,\text{Pipe}}(t) = \frac{\dot{m}_{i,\text{Pipe}}(t)}{\varrho_{i,\text{Pipe}}(t) A_{\text{Pipe}}}. \tag{5}$$

Note that $\dot{m}_{i,\text{Pipe}} = \dot{m}_{\text{feed}}$ is directly measured and $w_{i,\text{Pipe}} = w_{\text{feed}}$ is indirectly measured via $\varrho_{i,\text{Pipe}}$ and $\vartheta_{i,\text{P}}$, see App. A.

3.2 Plate

The Plate is a tank with a small gap at its bottom having the purpose to distribute the liquid uniformly over the Tube. In addition to that, so-called flash evaporation occurs if the liquid undergoes fast pressure reduction, i.e., if there is partial vacuum in the plant. To describe the input-output dynamics of the Plate, we use the same model as in (Schwaer et al. (2020); Ponomarev et al. (2020)):

$$\dot{m}_{\text{fsh}}(t) = \begin{cases} \frac{\dot{m}_{i,\text{P}}(t) c_p(t) (\vartheta_{i,\text{P}}(t) - \vartheta_{\text{T}}(t))}{(c_{p,\text{w}}(t) - c_p(t))\vartheta_{\text{T}}(t) + \Delta h_v(t)}, & \vartheta_{i,\text{P}} > \vartheta_{\text{T}}, \\ 0, & \text{else}, \end{cases} \tag{6}$$

$$\dot{m}_{\text{liq}}(t) = \dot{m}_{i,\text{P}}(t) - \dot{m}_{\text{fsh}}(t), \tag{7}$$

$$\frac{\mathrm{d}}{\mathrm{d}t}\dot{m}_{o,\text{P}}(t) = \frac{g \bar{\varrho}_{\text{P}}(t) A_{o,\text{P}}^2}{\dot{m}_{o,\text{P}}(t) A_{i,\text{P}}} \big(\dot{m}_{\text{liq}}(t) - \dot{m}_{o,\text{P}}(t)\big), \tag{8}$$

$$h_{\text{P}}(t) = \frac{1}{2g}\left(\frac{\dot{m}_{o,\text{P}}(t)}{\bar{\varrho}_{\text{P}}(t) A_{o,\text{P}}}\right)^2, \tag{9}$$

$$w_{\text{liq}}(t) = \frac{\dot{m}_{i,\text{P}}(t) w_{i,\text{P}}(t)}{\dot{m}_{\text{liq}}(t)}, \tag{10}$$

$$\frac{\mathrm{d}}{\mathrm{d}t} w_{o,\text{P}}(t) = \frac{\dot{m}_{\text{liq}}(t)}{\bar{\varrho}_{\text{P}}(t) A_{i,\text{P}} h_{\text{P}}(t)} \big(w_{\text{liq}}(t) - w_{o,\text{P}}(t)\big). \tag{11}$$

Since $\dot{m}_{\text{fsh}} \ll \dot{m}_{i,\text{P}}$, the average density $\bar{\varrho}_{\text{P}}$ between the input and output of the Plate can be approximated by the input density, i.e., $\bar{\varrho}_{\text{P}} \approx \varrho_{i,\text{P}}$.

3.3 Tube

The transport of $\dot{m}$ and w in the Tube is based on the OPF model, which describes overtaking of liquid particles by considering their velocity c as another independent variable in addition to space x and time t (Hofmann et al. (2020); Ponomarev et al. (2020)). A special feature of OPF is that, besides time-varying delay behavior, it allows diffusion modeling which is achieved by distributing the particles' velocities according to a probability-like distribution function. Thereafter, we consider the triangular distribution

$$f(c,t) = \begin{cases} \frac{2(c - c_{\min}(t))}{(\bar{c}(t) - c_{\min}(t))\Delta}, & c \in [c_{\min}(t), \bar{c}(t)], \\ \frac{2(c_{\max}(t) - c)}{(c_{\max}(t) - \bar{c}(t))\Delta}, & c \in (\bar{c}(t), c_{\max}(t)], \\ 0, & \text{else}, \end{cases} \tag{12a}$$

$$\Delta = c_{\max}(t) - c_{\min}(t), \tag{12b}$$

where

$$c_{\min}(t) = \frac{\ell}{\tau_{\max}(t)}, \tag{13a}$$

$$\bar{c}(t) = \frac{\ell}{\bar{\tau}(t)}, \tag{13b}$$

$$c_{\max}(t) = \frac{\ell}{\tau_{\min}(t)}. \tag{13c}$$

The triangular distribution function (12) with velocities (13) contains the three time-varying delay relations $\tau_{\min}(t)$, $\bar{\tau}(t)$, and $\tau_{\max}(t)$ to be identified in Sec. 4.

To model evaporation, we assume it proportional to the local amount of water in the Tube, i.e., where there is more water there is more evaporation. Observe that this evaporation model does not require any identification: It simply distributes the total mass flow of vapor proportionally to the local mass of water along the Tube. Without going into further details, we directly state the input-output dynamics obtained in (Ponomarev et al. (2020)):

$$\dot{m}_{o,\mathrm{T}}(t) = \int_{c_{\min}(t)}^{c_{\max}(t)} f(c,\sigma)\, \dot{m}_{i,\mathrm{T}}(\sigma) \Big[w_{i,\mathrm{T}}(\sigma) + \big(1 - w_{i,\mathrm{T}}(\sigma)\big)\beta(\sigma,t) \Big] \Big|_{\sigma=t-\ell/c} \mathrm{d}c, \tag{14}$$

$$w_{o,\mathrm{T}}(t) = \frac{1}{\dot{m}_{o,\mathrm{T}}(t)} \int_{c_{\min}(t)}^{c_{\max}(t)} f(c,\sigma)\, \dot{m}_{i,\mathrm{T}}(\sigma)\, w_{i,\mathrm{T}}(\sigma) \Big|_{\sigma=t-\ell/c} \mathrm{d}c, \tag{15}$$

where

$$\beta(\sigma,t) = \exp\left(-\int_{\sigma}^{t} b(\alpha)\,\mathrm{d}\alpha \right),\ b(t) = \frac{\dot{m}_{\mathrm{v}}(t)}{M_{\mathrm{w}}(t)}, \tag{16a}$$

$$\dot{m}_{\mathrm{v}}(t) = \frac{k\pi d\ell\big(\vartheta_{\mathrm{H}}(t) - \vartheta_{\mathrm{T}}(t)\big)}{\Delta h_v(t)}, \tag{16b}$$

$$M_{\mathrm{w}}(t) = \int_0^{\ell} \int_{c_{\min}(t)}^{c_{\max}(t)} f(c,\sigma)\, \dot{m}_{i,\mathrm{T}}(\sigma) \frac{\big(1 - w_{i,\mathrm{T}}(\sigma)\big)\beta(\sigma,t)}{c} \Big|_{\sigma=t-x/c} \mathrm{d}c\,\mathrm{d}x. \tag{16c}$$

In Fig. 4, a physical interpretation of the OPF delays $\tau_{\min}$, $\bar{\tau}$, and $\tau_{\max}$ is given by sketching the step-response of the OPF model without evaporation.

3.4 Reservoir

The Reservoir represents a tank receiving inflow from the Tube, while the outflow is generated by a downstream pump. Thus, the input-output behavior is modeled by

$$\dot{m}_{o,\mathrm{R}}(t) = \dot{m}_{o,\mathrm{T}}(t) - A_{\mathrm{R}} \left(h_{\mathrm{R}}(t) \frac{\mathrm{d}\varrho_{o,\mathrm{R}}(t)}{\mathrm{d}t} + \frac{\mathrm{d}h_{\mathrm{R}}(t)}{\mathrm{d}t} \varrho_{o,\mathrm{R}}(t) \right), \tag{17}$$

$$\frac{\mathrm{d}}{\mathrm{d}t} w_{o,\mathrm{R}}(t) = \frac{\zeta_{\mathrm{mix}} \dot{m}_{o,\mathrm{T}}(t)}{\varrho_{o,\mathrm{R}}(t) A_{\mathrm{R}} h_{\mathrm{R}}(t)} \big(w_{o,\mathrm{T}}(t) - w_{o,\mathrm{R}}(t) \big), \tag{18}$$

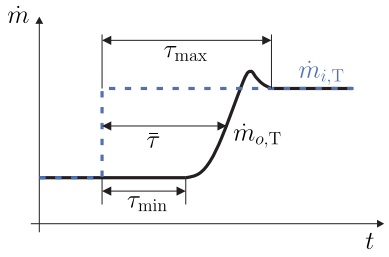

Fig. 4. OPF without evaporation: An input step affects a $\tau_{\min}$-delayed output reaction. After $\tau_{\max}$, all particles of the lower input flow arrive the output.

cf. (Schwaer et al. (2020)). Note that imperfect mixing of water and dry matter is considered by the factor $\zeta_{\mathrm{mix}} \in (0, 1]$, where $\zeta_{\mathrm{mix}} = 1$ corresponds to perfect mixing.

4. IDENTIFICATION

As mentioned in Sec. 2.2, circulation mode without evaporation is used for identification. By solving (17) w.r.t. $\dot{m}_{o,\mathrm{T}}$, we obtain

$$\dot{m}_{o,\mathrm{T}}(t) = \dot{m}_{o,\mathrm{R}}(t) + A_{\mathrm{R}} \left(h_{\mathrm{R}}(t) \frac{\mathrm{d}\varrho_{o,\mathrm{R}}(t)}{\mathrm{d}t} + \frac{\mathrm{d}h_{\mathrm{R}}(t)}{\mathrm{d}t} \varrho_{o,\mathrm{R}}(t) \right), \tag{19}$$

which shows that the mass flow out of the Tube is indirectly measured since all quantities on the right-hand side of (19) are measured or known. To keep numerical noise small, all derivatives in (19) are filtered via some basic moving average filter, where a window length of $T_{\mathrm{f}} = 3\,\mathrm{s}$ is sufficient. Hence, the corresponding signals are delayed by the average filter delay $\tau_{\mathrm{f}} = T_{\mathrm{f}}/2 = 1.5\,\mathrm{s}$. However, since τ_{f} is negligibly small compared to the OPF delays, a further investigation of its influence is not required. Summing up, the identification model is composed of (7), (8), (12), (13), (14) with $\beta(\sigma,t) = \dot{m}_{\mathrm{v}} = \dot{m}_{\mathrm{fsh}} \equiv 0$, $\varrho = \text{const.}$, and $w = \text{const.}$ In the sequel, we explicitly indicate modeled quantities by $\hat{(\cdot)}$, otherwise the quantity is measured.

4.1 Methodology

In order to use the maximum of information from available measurements, we identify the relations for the OPF delays $\tau_{\min}$, $\bar{\tau}$, and $\tau_{\max}$ by applying output error based least squares (Gröll (2015)) in the *offline* manner, i.e., identification is done *after* the experiment. Note that all other parameters apart from the OPF delays are either known by geometry or pre-identified in preliminary experiments. Firstly, we assume ansatzfunctions for the OPF delays to represent them as relations of flow and liquid properties. According to (Al-Sibai (2006); Åkesjö (2018)) and references therein, liquid film flow can be characterized via the Reynolds number defined by

$$Re(t) = \frac{\dot{m}_{i,\mathrm{T}}(t)}{\pi d \eta(t)} \tag{20}$$

such that identification of the ansatzfunctions

$$\tau_{\min}(t) = a_{\min} Re(t)^{b_{\min}}, \tag{21a}$$

$$\bar{\tau}(t) = \bar{a} Re(t)^{\bar{b}}, \tag{21b}$$

$$\tau_{\max}(t) = a_{\max} Re(t)^{b_{\max}} \tag{21c}$$

Table 2. Liquid properties of dextrose with polyvinylpyrrolidone for identification

No.	w in kg kg^{-1}	η in mPa s	ϱ in kg m^{-3}
1	0.42	43.053	1162
2	0.30	12.199	1107
3	0.14	2.2344	1039

Table 3. Identified parameters

No.	Re-range	$a_{\min}$	$b_{\min}$	$\bar{a}$	$\bar{b}$	$a_{\max}$	$b_{\max}$
1	[3.1, 6.1]	29.4	-0.25	80.3	-0.38	239.6	-0.054
2	[7.3, 19]	12.7	0.02	25.8	-0.11	42.1	-0.001
3	[40, 128]	8.94	-0.04	17.4	-0.03	58.4	-0.25

is convenient. Hence, the parameter vector is

$$\theta = \left[a_{\min},\, b_{\min},\, \bar{a},\, \bar{b},\, a_{\max},\, b_{\max}\right]^\top. \tag{22}$$

Secondly, we consider the output error

$$e_j = \dot{m}_{o,\mathrm{T}}(t_j;\theta) - \hat{\dot{m}}_{o,\mathrm{T}}(t_j;\hat{\theta}), \quad j = 1, 2, \ldots, N, \tag{23}$$

where $\dot{m}_{o,\mathrm{T}}$ is measured according to (19), $\hat{\dot{m}}_{o,\mathrm{T}}$ is the model output according to (14), and N denotes the number of samples. Note that the estimated parameter vector $\hat{\theta}$ is plugged into (14) via (13) and (21). The model and the pilot plant are both fed by the same measured input $\dot{m}_{i,\mathrm{P}}$. Furthermore, we consider the objective function

$$\min_{\hat{\theta}} \sum_{j=1}^{N} e_j^2, \tag{24}$$

which is minimized by some basic algorithm. In this contribution, we use the Matlab/Simulink implementation of the trust-region reflective algorithm.

4.2 Experiment Design

To identify $\hat{\theta}$, we apply three different mixtures of our test liquid, dextrose with polyvinylpyrrolidone, at the constant temperature $\vartheta_{i,\mathrm{P}} = \vartheta_{\mathrm{T}} = 60°\mathrm{C}$, see Table 2 and App. A. For each of these three mixtures, the following experiment is done:

(i) Operate the pilot plant in circulation mode.
(ii) Wait until the process is stationary, i.e., $\dot{m}_{i,\mathrm{P}} = \dot{m}_{o,\mathrm{R}} = \text{const.}$, $h_{\mathrm{R}} = \text{const.}$
(iii) By rapidly increasing/decreasing the pump's rotational speed, apply an up/down step to $\dot{m}_{i,\mathrm{P}} = \dot{m}_{o,\mathrm{R}}$ and measure the decrease/increase of h_{R}.
(iv) Repeat (ii) and (iii).
(v) Terminate the experiment when the mass flow range $\dot{m} \in [60, 120]\,\mathrm{kg\,h^{-1}}$ is covered by up/down steps.

Since there is no evaporation, the product properties w, η, and ϱ shown in Table 2 remain constant during each experiment (i)-(v).

4.3 Results

Table 3 shows the identified parameters for each experiment, where the numbering (No.) corresponds to the one in Table 2. Based on these parameters, Fig. 5 illustrates the OPF delays as functions of $\dot{m}_{i,\mathrm{T}}$ and η since the latter may vary during the real process with evaporation, cf. (20). The gaps between the identification data are interpolated via Matlab's `poly12`. As intuitively expected, the delays increase with increasing viscosity and decrease

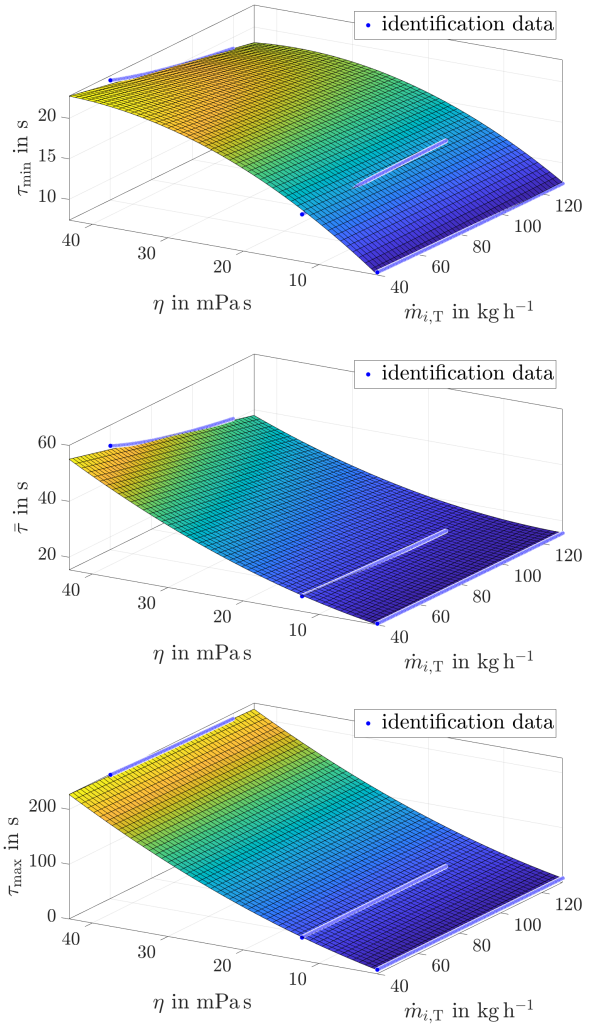

Fig. 5. Identified OPF delays as functions of $\dot{m}_{i,\mathrm{T}}$ and η

with increasing mass flow. Furthermore, we observe that the impact of viscosity on the delays is larger than the one of mass flow, in particular for $\tau_{\max}$.

Finally, the authors emphasize that all results are liquid-dependent and refer to dextrose with polyvinylpyrrolidone. If another liquid is considered, the results for the identified delays may differ from ours although they are valid in similar Re-ranges. The reason for this fact is that Re essentially relates $\dot{m}_{i,\mathrm{T}}$ to η, see (20), such that further liquid properties, like surface tension or thermal conductivity, remain unconsidered although they may affect the liquid's time-delay behavior. To solve this problem, there exists the option to include additional characteristic numbers, such as Kapitza or Prandtl number, into the ansatzfunctions (21), cf. (Jani (2012)). However, in this case, the identification effort is increased and additionally, relations for the further liquid properties have to pre-identified in preliminary experiments. Due to these drawbacks, we restrict the identification to Re since it is the most significant characteristic number to investigate liquid film flow (Al-Sibai (2006)). Anyway, we keep the limitations of our approach in mind and recommend to repeat our time-delay identification methodology if other test liquids are considered.

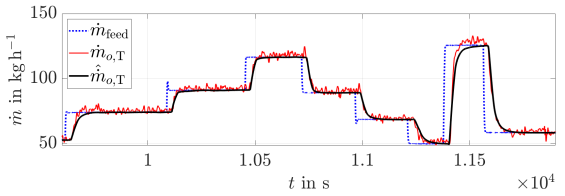

(a) $w = 0.45\,\text{kg kg}^{-1}$

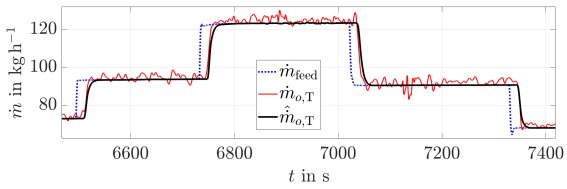

(b) $w = 0.30\,\text{kg kg}^{-1}$

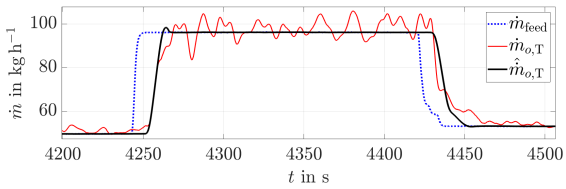

(c) $w = 0.15\,\text{kg kg}^{-1}$

Fig. 6. Validation without evaporation

5. VALIDATION

In this section, we test our identified model in validation experiments. Since real FFEs usually operate in single pass mode, see Sec. 2.3, we validate our models in this mode.

In the first step, we conduct a validation experiment without evaporation. To this end, similar step-experiments as described under (ii)-(iv) in Sec. 4.2 are applied. The corresponding results are depicted in Fig. 6. As delays get smaller with decreasing dry matter content w, the scale is correspondingly adapted in each subfigure of Fig. 6. To sum up, we can see that model and experiment are in very good accordance.

In the second step, we additionally apply evaporation and therefore have real FFE process conditions. Hence, besides mass flow $\dot{m}_{o,\text{T}}$, the dry matter content $w_{o,\text{R}}$ is another important output. The results of this experiment are shown in Fig. 7. From the plots for $\dot{m}$, it follows that the influence of evaporation on the liquid film's time-delay behavior is negligible since $\dot{m}_{o,\text{T}}$ and $\hat{\dot{m}}_{o,\text{T}}$ still coincide well although the OPF delays were identified in experiments without evaporation. In other words, the increase of the liquid's dynamic viscosity η and density ϱ due to evaporation does not significantly affect the time delay behavior.

Similarly, the validation of dry matter content w also reveals that model and experiment are in good accordance. The only remarkable deviation is observed in Fig. 7b during $t \in [2400, 2680]\,\text{s}$. The reason for this deviation is the calculation of $\hat{\dot{m}}_{\text{v}}$ via (16b), where we assume constant k-values (thermal conductivity). According to (Winchester (2000); Ponomarev et al. (2020)), the k-values decrease with increasing w since heat transfer

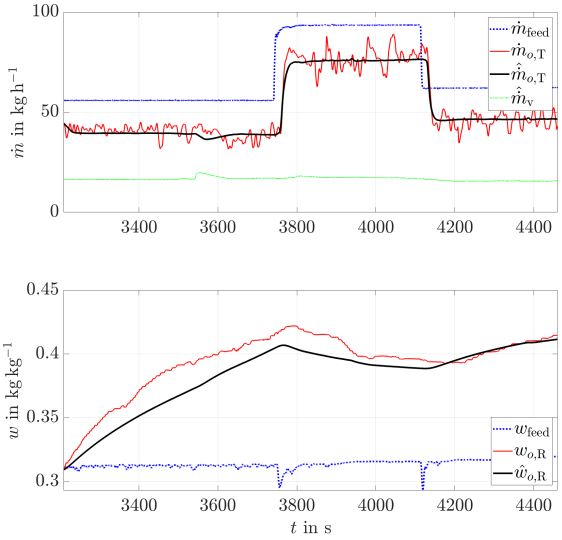

(a) $w_{\text{feed}} = 0.30\,\text{kg kg}^{-1}$

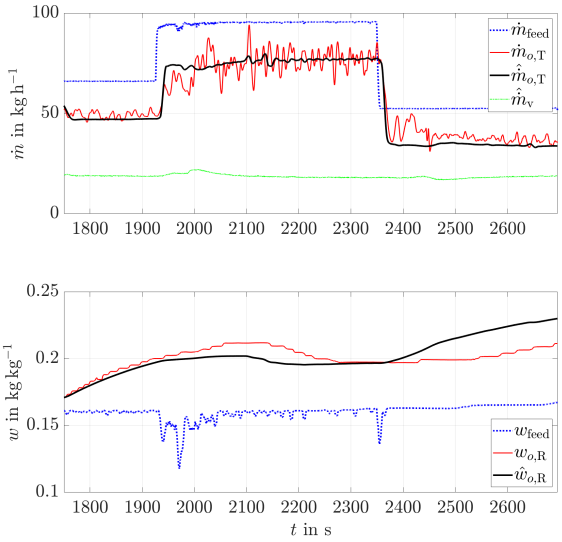

(b) $w_{\text{feed}} = 0.15\,\text{kg kg}^{-1}$

Fig. 7. Validation with evaporation

worsens. Thus, as our model assumes constant k-values, we overestimate evaporation a bit during the aforementioned time span. Nevertheless, this simplification mostly models evaporation well enough as shown by Fig. 7a, where $w_{o,\text{R}}$ and $\hat{w}_{o,\text{R}}$ are in very good agreement. Broadly speaking, our model is well capable to describe the real FFE process and therefore is considered to be validated.

6. CONCLUSIONS AND OUTLOOK

This paper presents an offline time-delay identification strategy based on falling film evaporator pilot plant experiments. Although the delay relations are identified in experiments without evaporation, they yield good results in both of the validation experiments, with and without evaporation, see Fig. 6 and Fig. 7. Thus, we conclude that the influence of evaporation on the liquid's time-delay behavior can be neglected while dynamic viscosity

and mass flow are decisive, which is evident in Fig. 5. Since evaporation generally increases the liquid's dynamic viscosity, the aforementioned conclusion may, at first sight, sound contradictory to the reader. However, the increase of dynamic viscosity due to evaporation is comparatively small as the liquid flows down the Tube. This fact can be regarded as descriptive explanation why the influence of evaporation does not need to be taken into account when considering the liquid's time-delay behavior. To give an outlook, future work on online time-delay estimation techniques is desirable as the identification results of this contribution are liquid-dependent and require quite large effort.

REFERENCES

Åkesjö, A. (2018). *Hydrodynamics and heat transfer in vertical falling films with smooth and modified heat-transfer surfaces: an experimental and numerical investigation*. Department of Chemistry and Chemical Engineering, Chalmers University of Technology.

Al-Sibai, F. (2006). *Experimentelle Untersuchung der Strömungscharakteristik und des Wärmeübergangs bei welligen Rieselfilmen*. Cuvillier Verlag.

Bresch-Pietri, D. and Petit, N. (2016). Implicit integral equations for modeling systems with a transport delay. In *Recent Results on Time-Delay Systems*, 3–21. Springer.

Craster, R. and Matar, O. (2009). Dynamics and stability of thin liquid films. *Reviews of Modern Physics*, 81(3), 1131.

Donaldson, A. and Thimmaiah, A. (2016). Process modelling and optimization of design parameters in a falling film plate and frame evaporator. In *Proceedings of the COMSOL Conference*, 1–9.

Gröll, L. (2015). *Methodik zur Integration von Vorwissen in die Modellbildung*, volume 52. KIT Scientific Publishing.

Hofmann, J., Ponomarev, A., Hagenmeyer, V., and Gröll, L. (2020). Transport models for liquid films (in German). *at - Automatisierungstechnik*, 68(8), 625–640.

Jani, S. (2012). Simulation of heat and mass transfer process in falling film single tube absorption generator. *International Journal of Science and Engineering Investigations*, 1(3), 79–84.

Karafyllis, I. and Krstic, M. (2014). On the relation of delay equations to first-order hyperbolic partial differential equations. *ESAIM: Control, Optimisation and Calculus of Variations*, 20(3), 894–923.

Karapantsios, T. and Karabelas, A. (1995). Longitudinal characteristics of wavy falling films. *International Journal of Multiphase Flow*, 21(1), 119–127.

Keyhani, M. (2001). The effect of roll waves on the hydrodynamics of falling films observed in vertical column absorbers. In *Proceedings of the ASME Advanced Energy Systems Division*, 45. American Society of Mechanical Engineers.

Kharangate, C.R., Lee, H., and Mudawar, I. (2015). Computational modeling of turbulent evaporating falling films. *International Journal of Heat and Mass Transfer*, 81, 52–62.

Paramalingam, S. (2004). *Modelling, optimisation and control of a falling-film evaporator*. Ph.D. thesis, Massey University, New Zealand.

Ponomarev, A., Hofmann, J., and Gröll, L. (2020). Novel control-oriented models for liquid transport in falling film evaporator tubes. Submitted for publication.

Schwaer, C., Hofmann, J., Mühlpfordt, M., Frank, A., and Gröll, L. (2020). Modular simulation model for falling film evaporators with novel approach to manage dominant time-varying transport delays. *Computers & Chemical Engineering*, 132, 106604.

Van Genuchten, M.T. (1982). *Analytical solutions of the one-dimensional convective-dispersive solute transport equation*. 1661. US Department of Agriculture, Agricultural Research Service.

Winchester, J. (2000). *Model based analysis of the operation and control of falling-film evaporators*. Ph.D. thesis, Massey University, New Zealand.

Witrant, E. and Niculescu, S.I. (2010). Modeling and control of large convective flows with time-delays. *Mathematics in Engineering, Science and Aerospace*, 1(2), 191–205.

Zenger, K. and Ylinen, R. (1994). Simulation of variable delays in material transport models. *Mathematics and Computers in Simulation*, 37(1), 57–72.

Zhang, F. and Yeddanapudi, M. (2012). Modeling and simulation of time-varying delays. In *Theory of Modeling and Simulation-DEVS Integrative M&S Symposium*, 34. Society for Computer Simulation International.

Appendix A. LIQUID PROPERTIES

The properties of our test liquid, dextrose with polyvinylpyrrolidone, are given in Table 4. In this context, the variables ϑ and w, which are both functions of time t, should be chosen according to the sensor which is closest to the place of interest in the plant. For convenience, we defined all liquid properties simply as functions of t throughout the paper but, in this appendix, we specify them for each relevant equation:

- In (5): $\varrho_{i,\mathrm{Pipe}}(t) := \varrho(w_{\mathrm{feed}}, \vartheta_{i,\mathrm{P}})$.
- In (6): $c_p(t) := c_p(\vartheta_{\mathrm{T}}, w_{i,\mathrm{P}})$, $c_{p,\mathrm{w}}(t) := c_{p,\mathrm{w}}(\vartheta_{\mathrm{T}})$, $\Delta h_v(t) := \Delta h_v(\vartheta_{\mathrm{T}})$.
- In (8), (9), (11): $\bar{\varrho}_{\mathrm{P}}(t) \approx \varrho_{i,\mathrm{P}}(t) := \varrho(w_{i,\mathrm{P}}, \vartheta_{i,\mathrm{P}})$.
- In (16b): $\Delta h_v(t) := \Delta h_v(\vartheta_{\mathrm{T}})$.
- In (17)-(19): $\varrho_{o,\mathrm{R}}(t) := \varrho(w_{o,\mathrm{R}}, \vartheta_{i,\mathrm{P}})$.
- In (20): $\eta(t) := \eta(w_{i,\mathrm{P}}, \vartheta_{\mathrm{T}})$.

Table 4. Liquid properties of dextrose with polyvinylpyrrolidone

Param.	Formula	Constants
$\varrho(\vartheta, w)$	$\underbrace{\left(\mathrm{A_w} + \mathrm{B_w}\frac{\vartheta}{\mathrm{K}} + \mathrm{C_w}\frac{\vartheta^2}{\mathrm{K}^2}\right)\frac{\mathrm{kg}}{\mathrm{m}^3}}_{=\varrho_\mathrm{w}(\vartheta)}\left(1 + \mathrm{A}w^\mathrm{B}\right)$	$\mathrm{A_w} = 629.498$ $\mathrm{B_w} = 2.64029$ $\mathrm{C_w} = -0.0047$ $\mathrm{A} = 0.368857$ $\mathrm{B} = 0.137827$
$\Delta h_v(\vartheta)$	$\mathrm{B}\left(\frac{1-\frac{\vartheta}{\mathrm{C}}}{1-\frac{\mathrm{A}}{\mathrm{C}}}\right)^{0.38}\frac{\mathrm{kJ}}{\mathrm{kg}}$	$\mathrm{A} = 323.15$ $\mathrm{B} = 2382$ $\mathrm{C} = 0.324$
$c_p(\vartheta, w)$	$(\mathrm{A} + \mathrm{B}\vartheta)\,w\frac{\mathrm{kJ}}{\mathrm{kg}\cdot\mathrm{K}} + \underbrace{\left(\mathrm{A_w} + \mathrm{B_w}\vartheta + \mathrm{C_w}\vartheta^2\right)\frac{\mathrm{kJ}}{\mathrm{kg}\cdot\mathrm{K}}}_{=c_{p,\mathrm{w}}(\vartheta)}(1-w)$	$\mathrm{A_w} = 5.647$ $\mathrm{B_w} = -0.00905$ $\mathrm{C_w} = 1.4 \cdot 10^{-5}$ $\mathrm{A} = 7.266476$ $\mathrm{B} = -0.016612$
$\eta(\vartheta, w)$	$\exp\left(\mathrm{E} + \frac{\mathrm{F}}{\mathrm{C}w+1} + \mathrm{A}w^\mathrm{D} - (\mathrm{B}w + \mathrm{G})(\vartheta - \vartheta_\mathrm{amb})\right)\mathrm{Pa}\cdot\mathrm{s}$	$\mathrm{A} = 11.248094$ $\mathrm{B} = 0.021970$ $\mathrm{C} = 0.123447$ $\mathrm{D} = 0.983533$ $\mathrm{E} = -5.703782475$ $\mathrm{F} = -1.203972904$ $\mathrm{G} = 0.018$ $\vartheta_\mathrm{amb} = 293.15\,\mathrm{K}$